Design and Test of SiPM Structures in CMOS Technology

N. D'Ascenzo[1,2], V. Saveliev[1,2] and Q. Xie[1,2]

[1]*Hiazhong University of Science and Technology, Wuhan, China*

[2]*Wuhan National Laboratory for Optoelectronics, Wuhan, China*

Keywords: Silicon Photomultiplier, Avalanche Breakdown Structures, CMOS.

Abstract: In this paper we report our results on the influence of STI guard ring structures on the design and performances of SiPM with n+p microcells. Two types of SiPM detection structures were designed and fabricated in standard CMOS technology production line. A key-point of our study is the mathematical modelling and simulation of the structure using the well-estabilished CMOS technology simulation frameworks and models. We analyse the electric field and ionization coefficients of the designed structures at breakdown voltage. In addition, experimental characterization of the fabricated SiPM including current characteristics, CV characteristics was measured and analysed in order to identify the best structure for a correct CMOS implementation of the SiPM with STI guard rings.

1 INTRODUCTION

The Silicon Photomultiplier (SiPM) had an impressive development in the last decade ((Saveliev and Golovin, 2000; Saveliev, 2010; D'Ascenzo and Saveliev, 2012; D'Ascenzo et al., 2015; Golovin and Saveliev, 2004)). It is a semiconductor detector consisting of an array of space-distributed micro-sensors. Each micro-sensor is capable of detecting a single quantum of light and the array is detecting a photon flux. The structure of a micro-cell is based on a n^+p or p^+n junction operated in avalanche breakdown mode.

A resistor is placed in series of each micro-sensor, integrated in the chip, in order to passive quench the avalanche. The miniature size of 1 mm^2, the high achievable density of microcells of approximately 1000/mm^2, the low bias voltage, the radiation hardness and insensitivity to the magnetic field satisfy the operational conditions of a variety of applications ranging from High Energy Physics to Homeland Security and Nuclear Medicine. Similar structures are also known as arrays of large number of single photon avalanche diodes (SPAD) (Charbon et al., 2013; Charbon, 2012; Zappa et al., 2007).

The recent advances in the conception of the SiPM are based on the investigation of the possibility of a full implementation of the photo-detector within standard CMOS. The SiPM design is in fact compatible with the standard available CMOS technology. The implementation of the SiPM in standard CMOS technology enables the monolithic integration of readout electronics and photo-detector on the same chip, with significant reduction of power consumption and simplification of the operational conditions. Further progress and development of even more sophisticated detector concepts will be also enabled by this possibility. Based on this idea an innovative position sensitive pixelated sensor for the detection and measurement of the coordinates of ionising particles with high precision has been proposed (D'Ascenzo et al., 2014). The silicon avalanche pixel sensor (APiX) is based on the vertical integration of avalanche pixels connected in pairs and operated in coincidence in fully digital mode and with the processing electronics embedded on the chip. Moreover the use of standard CMOS technology facilities would in fact reduce the cost of the detector, allowing an effective and stable mass production for industry use.

However, SiPM can suffer of localized breakdown conditions on the locally concentrated high electric field at the junction edges. The use of guard ring structures around the sensitive area of each microcell is in this respect mandatory in order to obtain a uniform electric field across the whole sensitive area. The CMOS technology offers few possibilities of implementing such guard rings ((ITRS, 2003; Lee et al., 2012; Izhaky et al., 2006)). It is possible to surround the highly doped n+ or p+ areas with a weakly doped n- or p- well in order to smooth the resulting electric field at the edge of the junction. It is also possi-
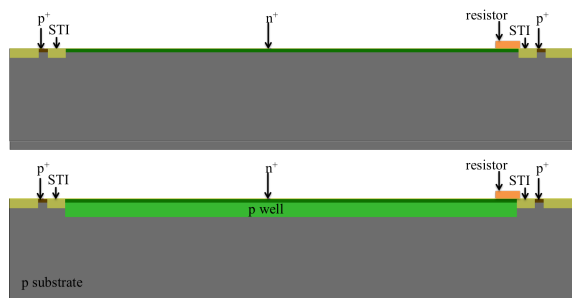
Figure 1: Cross section of the two types of SIPM structures in 180 nm CMOS technology: n^+/psub structure (up) and n^+/pwell (down). Both structures are with STI guard rings.

ble to use Shallow Trench Isolation (STI) around the highly doped n+ or p+ areas in order to remove the discontinuity in doping concentration at the edges of the structure.

In this paper we report our results on the influence of STI guard ring structures on the design and performances of SiPM on the example of n+p microcell structure. Two types of SiPM detection structures were designed and fabricated in standard CMOS technology production line. Using mathematical modelling and simulation, we analyse their electric field and ionisation coefficients at breakdown voltage . In addition, experimental characterisation of the fabricated SiPM including current characteristics, CV characteristics was measured and analysed in order to identify the best structure for a correct CMOS implementation of the SiPM with STI guard rings.

2 DEVICE STRUCTURES AND SIMULATION RESULTS

The cross sections of the two types of SiPM structures fabricated in 180 nm CMOS technology are shown in Fig. 1. The first structure consists of a np junction formed with an n^+ implantation on the silicon substrate. The second structure consists of a np junction formed with an n^+ implantation on a p-well. STI guard rings are placed around the n^+ implantation, between the n^+ and p^+ implantation, according to the standard CMOS rules. The output current from the junction flows through a quenching resistor with typical value ranging between 500 kΩ and 1 MΩ. The resistor is obtained with High Resistive Polysilicon (HRP) technology also available at CMOS foundry. The sensitive area consists of a $50 \times 50 \ \mu m^2$ window, corresponding to the n^+ implantation. The design follows strongly the design rules of the 180 nm CMOS technology used for design and production.

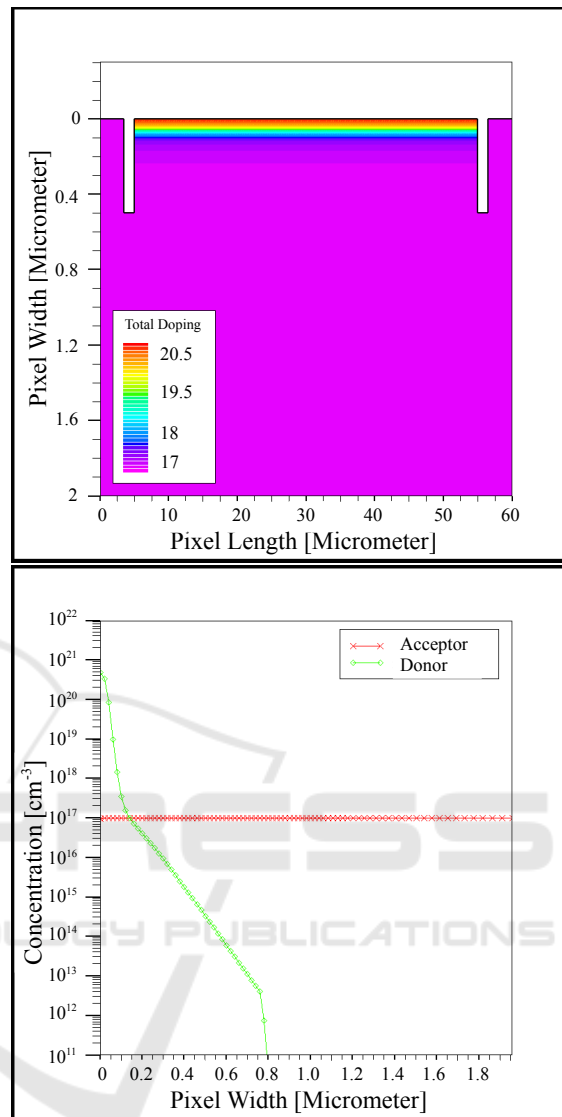We perform the device mathematical modelling

Figure 2: Total doping profiles of the simulated n^+/psub structure. Transverse view (top panel) and cross sectional view along the central line at length 30 μm (bottom panel).

within the simulation framework SILVACO (Silvaco). The aim of the mathematical model is the extraction of the influence of the STI guard rings on the electric field profiles for both structures of the CMOS SiPMs. The doping profiles are obtained with a detailed device process simulation, corresponding to the indications of the production facility.

The cross sectional view and the profile of the total doping of the n^+/psub and n^+/pwell structures is shown on Fig. 2, 3. The doping concentration of the p-substrate is about 10^{17} cm^{-3}, The obtained p-well concentration ranges between 10^{17} cm^{-3} at the surface and a maximal value of about 4.5×10^{17} cm^{-3} at a depth of 0.6 μm. The concentration of the n^+ im-
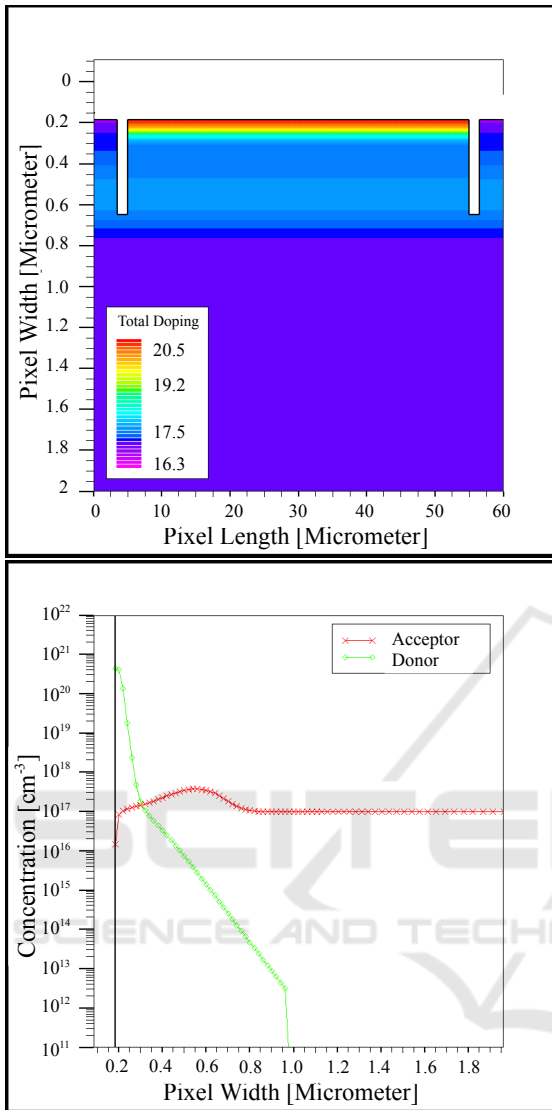
Figure 3: Total doping profiles of the simulated n^+/pwell structure. Transverse view (top panel) and cross sectional view along the central line at length 30 μm (bottom panel).

plantation peaks at 4×10^{21} cm^{-3}.

The simulation of the DC and AC device includes the solution of the Boltzmann transport equation, including the auger recombination model and the Selberherr's model (Sze and K.N., 2007) for the description of the impact ionisation process. The Poisson equation is solved dynamically for the determination of the strength of the electric field across the junction.

The numerical simulation allows studying the effects of localised breakdown conditions due to the local geometry of the junction and allows designing the guard rings structures for the correction of such problem.

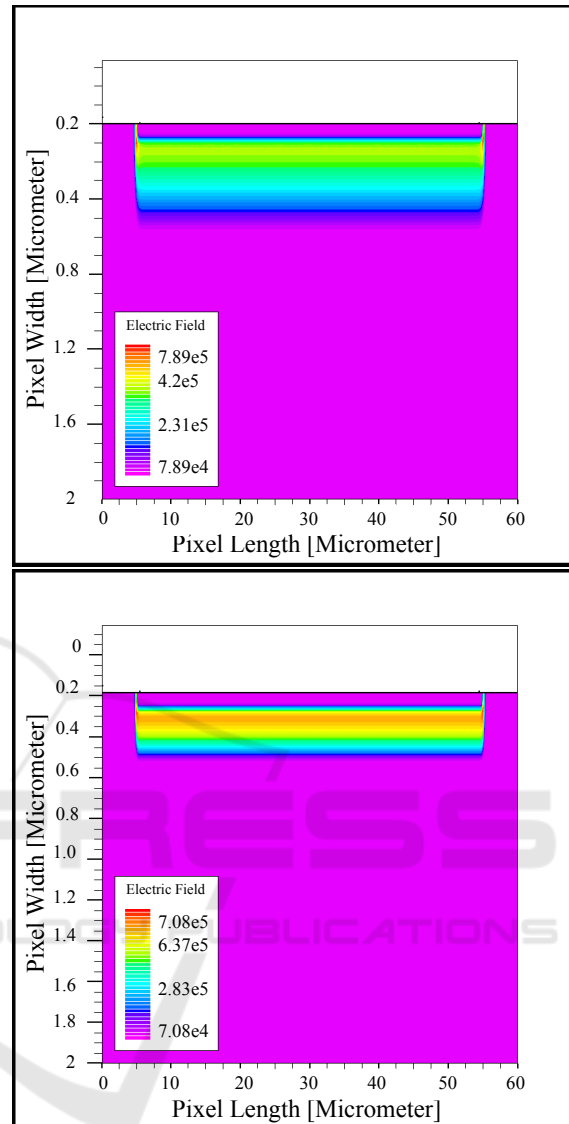As an example, we first study the properties of

Figure 4: Electric field strength of the simulated n^+/psub(top) and n^+/pwell (bottom) structure without STI. The non uniformity of the electric field on the corners of the junction is visible.

the detection structures without STI. The cross sectional view of the electric field at breakdown across the junction for both structures without STI is shown on Fig. 4. The electric field without STI exhibits an upper value respectively of about 8×10^5 V/cm in both structures on a localised spot at the junction corners. The strength of the electric field along the junction is uniform with a value of about respectively 4.5×10^5 V/cm and 6×10^5. Thus, in a structure without STI trenches, the electric field strength on the junction periphery exceeds of a factor 2 the electric field strength along the sensitive area of the diode, causing strong non-uniformity in light detection ef-
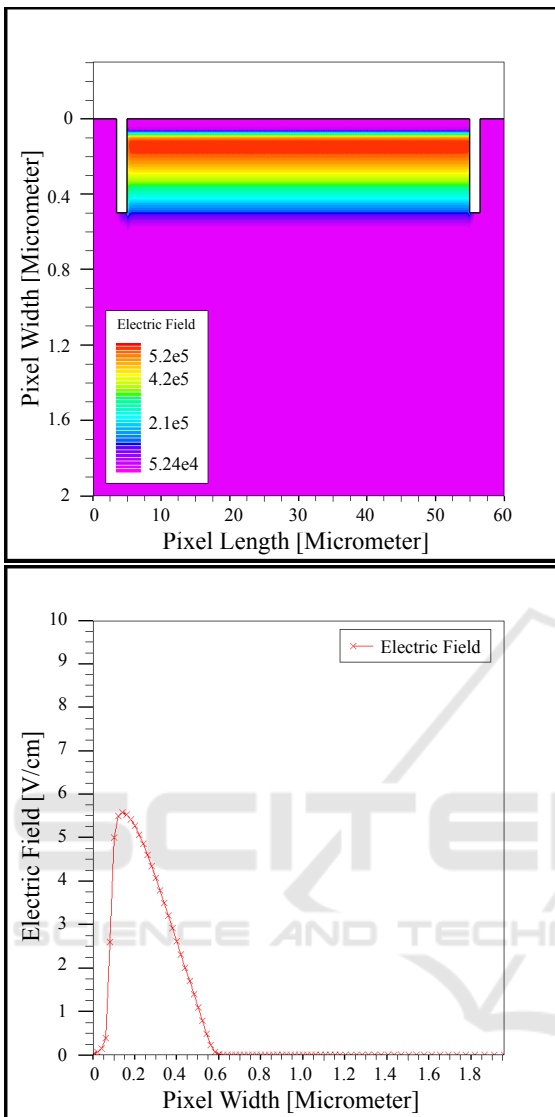
Figure 5: Electric field strength of the simulated n^+/psub structure. Transverse view (top panel) and cross sectional view along the central line at length 30 μm (bottom panel).
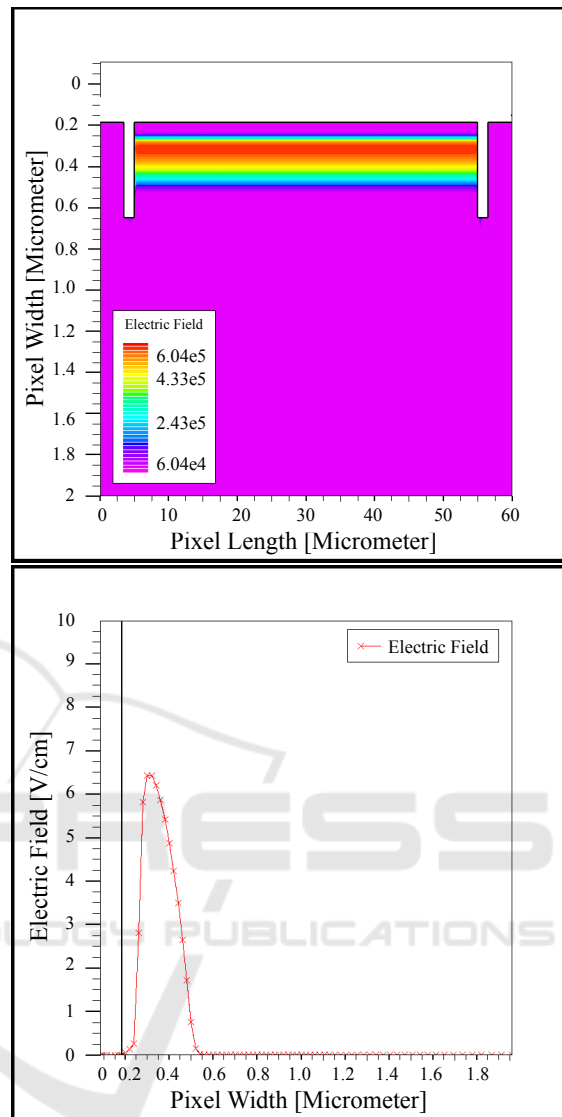

Figure 6: Electric field strength of the simulated n^+/pwell structure. Transverse view (top panel) and cross sectional view along the central line at length 30 μm (bottom panel).

ficiency. In other words, the dominant sensitive part reduces in this case only to the edges of the junction.

The introduction of the STI guard rings improves the situation significantly. The cross sectional view and the profile of the electric field across the junction at breakdown is shown in Fig. 5, 6 respectively for the n^+/psub and n^+/pwell structures at their respective breakdown voltage. The corner effect at the edges of the junction disappears and the electric field is uniform along the whole junction. The maximal electric field obtained with the n+/psub structure is about 5.5×10^5 V/cm at about 0.2 μm from the surface, while the maximal electric field obtained with the n+/pwell structure is about 6.4×10^5 V/cm at

about 0.1 μm from the surface.

From a comparison between Fig. 5 and Fig. 6 we observe that, due to the lower doping concentration of the n^+/psub structure respect to the n^+/pwell structure, the junction width of the first structure is wider than the second one, being the widths respectively about 0.5 μm and 0.3 μm.

The working principle of the SiPM is the passive quenching. The voltage drop through a quenching resistor causes the bias on the diode to decrease and stops the avalanche process occurring in the junction. This is in opposition with the traditional avalanche photodiodedes, which are operated in a self-quenching mode, though statistical fluctuation of
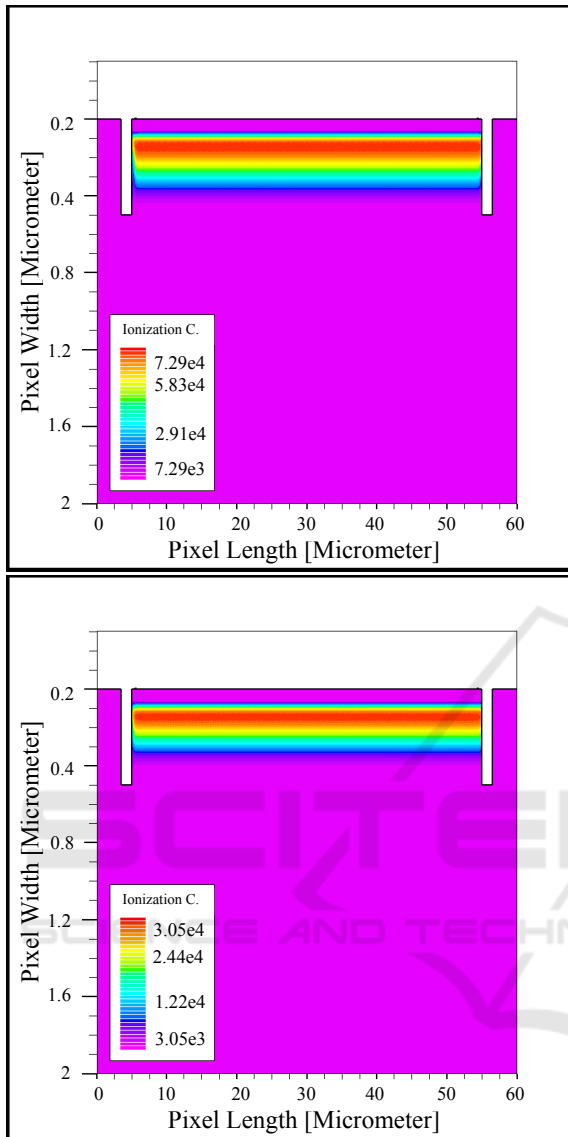
Figure 7: Impact ionisation coefficient for electron (top) and holes (bottom) in n$^+$/psub structure.

Figure 8: Impact ionisation coefficient for electron (top) and holes (bottom) in n$^+$/pwell (bottom) structure.

the avalanche. In other words, the gain of a SiPM is determined uniquely by the quenching resistor. It is thus needed to operate the detector in a regime, where both carriers contribute to the avalanche process, in order to develop a self-sustaining avalanche. In other words the ionisation coefficient of both electrons and holes needs to be of the same order of magnitude for a correct operation of the SiPM.

The ionisation coefficient for electron and holes is calculated in the simulation and is shown on Fig. 7, Fig 8 and Fig. 9 for respectively the n$^+$/psub and n$^+$/pwell structures.

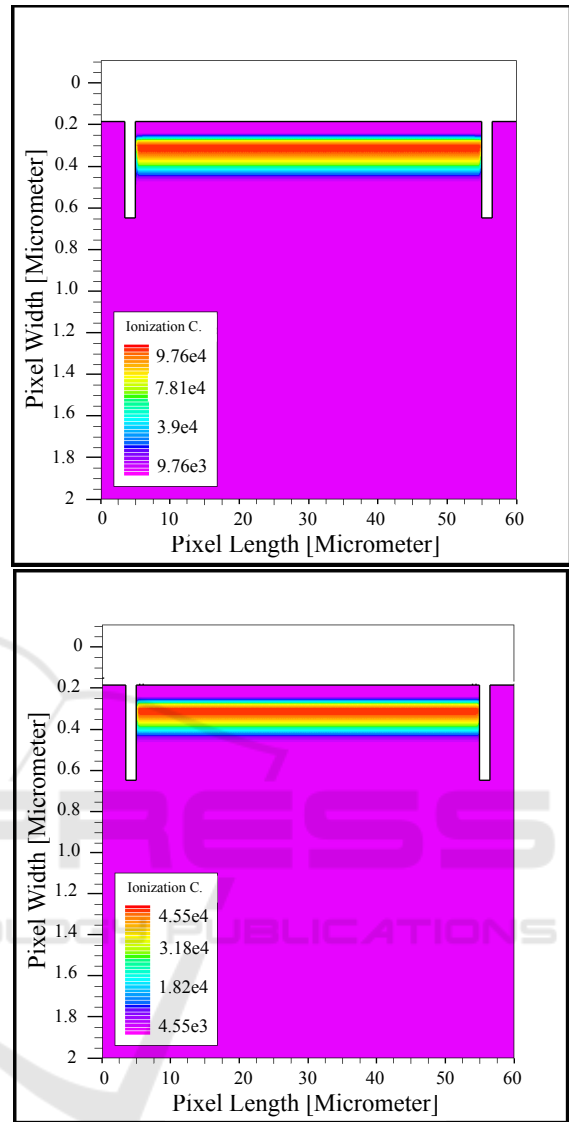In correspondence with the electric field, the ionisation coefficient of electron and holes is uniform along the junction for both structures. At the breakdown, the maximal value of the ionisation coefficient of electron and holes in the n$^+$/psub structure is respectively about 7.8×10^5 and 3.2×10^5, while in the n$^+$/pwell structure it reaches respectively 1.1×10^6 and 5×10^5. The comparison between the two structures allows to conclude that at the breakdown the impact ionisation of the n$^+$/psub is slightly lower than the impact ionisation for the he n$^+$/pwell structure. In fact the electric field strength is slightly lower in the first case. Moreover, we observe that in both structures the electron and holes ionisation coefficient is of the same order of magnitude, the holes ionisation coefficient being smaller than the electrons one. Thus, we suggest to optimise the stabilisation of the detec-
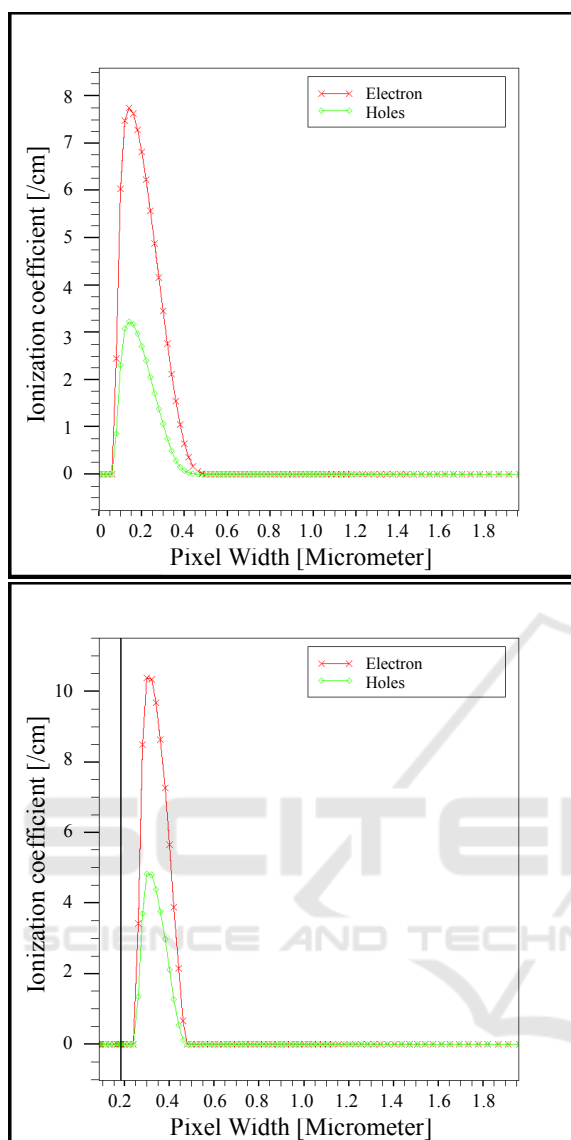
Figure 10: Mathematical modelling: IV characterisation of the SiPM structures.

Figure 9: Impact ionisation coefficient for electron and holes in n^+/psub(top) and n^+/pwell (bottom) structure.
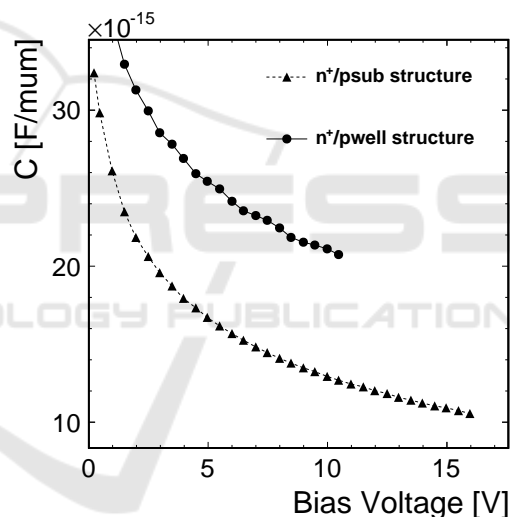
Figure 11: Mathematical modelling: CV characterisation of the SiPM structures.

tor operation in both structures at least 1 V above the breakdown voltage, in order to further increase the ionisation coefficient of the holes. Such region is out of reach for the mathematical model implemented here, and in the real application is achieved with a stabilisation of the SiPM through the passive quenching mechanism.

The IV characterization of the structure is shown on Fig 10 for both structures under analysis. The n^+/psub structure exhibits a breakdown at around 15.5 V, while the the n^+/psub structure exhibits a breakdown at around 10.5 V. The higher breakdown voltage of the n^+/psub is due to the lower average concentration of the p substrate in comparison with
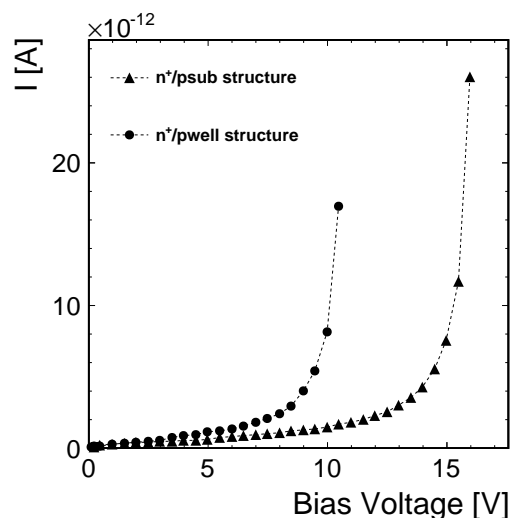
the well concentration.

Finally the CV characterisation of the structure is shown on Fig. 11 for both structures under analysis. The capacitance of the structures is calculated in an ac analysis at 1 kHz until the breakdown voltage of the structure is reached. We observe that the capacitance of the n^+/psub structures is lower than the capacitance of the n^+/pwell structures of approximately a factor 2 at the breakdown voltage. This corresponds to the observation that the width of the junction is in the n^+/psub structure is approximately twice as larger as in the n^+/pwell structure.

3 EXPERIMENTAL RESULTS

SiPM detectors were designed and fabricated in a standard 180 nm CMOS process on Multi Project Wafer according to the detector structures shown in the previous section. The obtained photodetectors consist of a 1 mm^2 array of microcells. Each microcell has a sensitive area of 50 μm. Two different samples on the basis of n$^+$/psub and n$^+$/pwell structures were fabricated. DC and AC measurements were performed on wafer after production in a controlled optical setup allowing for a characterisation in controlled dark environment.

The IV curves measured in dark condition for the n$^+$/psub and n$^+$/pwell SiPM are shown on Fig. 12.

We measure a breakdown voltage respectively of 15.5 V and 10.5 V, which confirms the prediction of the mathematical model and simulation.

We observe that the n$^+$/pwell structure exhibits enhanced dark current than the n$^+$/psub structure. This is probably due to enhanced tunnelling effects at the edges between the well and the STI. Further investigation is needed in order to understand these additional components of the dark current in well structures. However, the dark current level is well below the breakdown current. After the breakdown voltage, the quenching resistor acts as a current limiter, affecting the slope of the IV curve and stabilising the SiPM response. The enhancement of the dark current in n$^+$/pwell structures could hence impact on the single photon resolution only on a limited extent, causing only an higher expected dark rate of the device.

The CV characterization of the photodetectors at 1 kHz is shown on Fig. 13. The capacitance at breakdown is measured respectively as 0.15×10^{-9} F and 0.3×10^{-9} F for the n$^+$/psub and the n$^+$/pwell structures. Although the absolute value of these numbers refer to the full array of microcells and can not be compared with the simulation results, the relative strength of the capacitance in the two cases is in agreement with the mathematical model expectation. In fact we observe that the ration between the capacitance at breakdown for the two junctions is approximately a factor 2, which agrees with the mathematical model estimation of the difference in the junction width.

4 CONCLUSIONS

The work presented in this paper shows a step in the implementation of Silicon Photomultiplier structures in the standard CMOS technology. We show that both
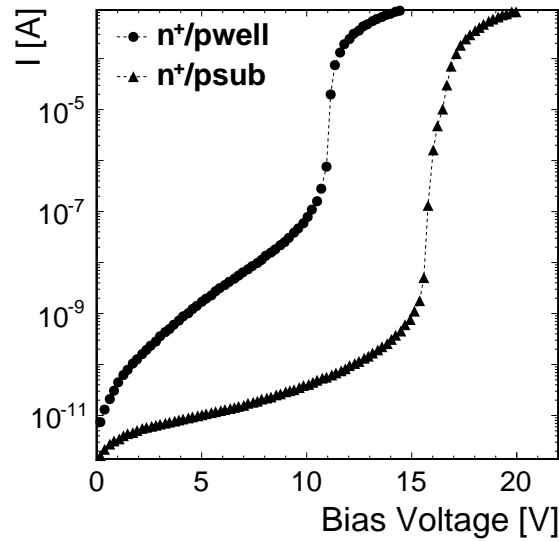

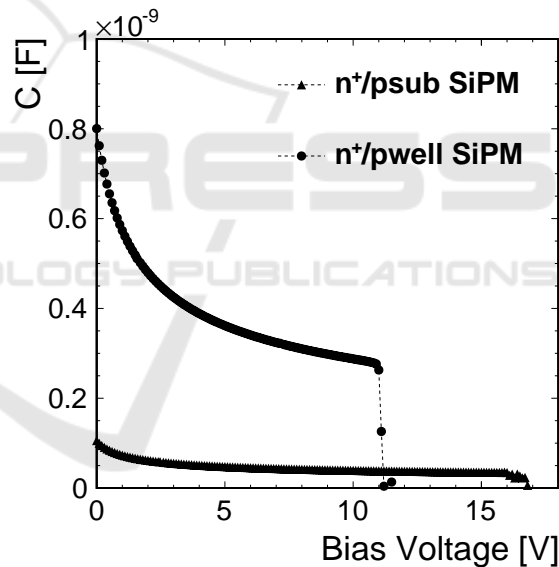Figure 12: Experimental measurement: IV characterisation of the SiPM structures.

Figure 13: Experimental measurement: CV characterisation of the SiPM structures.

the n$^+$/psub and n$^+$/pwell structures with STI based guard rings are both possible candidates for the design of a performant photodetector, in terms of geiger mode avalanche breakdown operation.

A particular interesting result of this study is that the production process and the results may be studied with solid mathematical modelling and simulation developed and used in the standard CMOS technology. Furthermore the development and design is performed on the basis of CMOS Multi Project Wafer (MPW). We find that the mathematical model predicts

very precisely the obtained experimental results and can be used as a solid tool for the design and development of the CMOS based SiPM.

The results of the experimental tests show the progress of the implementation of the SiPM in standard CMOS technology and opens the way and opportunity of novel intelligent and optimised design of this photodetector.

ACKNOWLEDGEMENTS

REFERENCES

Charbon, E. (2012). Single photon imaging in complementary metal oxide semiconductor processes. *Phyl. Trans. R. Soc. A*, 372:20130100.

Charbon, E., Fishburn, M., Walker, R., Henderson, R., and Niclass, C. (2013). *SPAD-Based Sensors*. In F. Remondino and D. Stoppa (eds.) TOF Range Imaging Cameras, Springer Verlag, 1st edition.

D'Ascenzo, N., Marrocchesi, P., Moon, C., Morsani, F., Ratti, L., Saveliev, V., Savoy-Navarro, A., and Xie, Q. (2014). Silicon avalanche pixel sensors for high precision tracking. *JINST*, 9:C03027.

D'Ascenzo, N. and Saveliev, V. (2012). *The new photodetectors for High Energy Physics and Nuclear Medicine*. In : Jin-Wei Shi (Ed.) Photodiodes-Communications, Bio-Sensing, Measurements and High Energy Physics, Intech, ISBN:978-953-307-277-7, 1st edition.

D'Ascenzo, N., Saveliev, V., Xie, Q., and Wang, L. (2015). *The digital silicon photonultiplier*. In: Ed. S.L.Pyshkin and J. Ballato, Optoelectronics - Materials and Devices, Intech, ISBN: 978-953-51-2174-9, 1st edition.

Golovin, V. and Saveliev, V. (2004). Novel type of avalanche photodetector with geiger mode operation. *Nuclear instruments and methods A*, 518:560–564.

ITRS (2003). Process integration, devices and structure summary. Technical report.

Izhaky, N., Morse, M., Koehl, S., Cohen, O., Rubin, D., Barkai, A., Savid, G., Corhen, R., and Paniccia, M. (2006). Development of cmos-compatible integrated silicon photonics devices. *IEEE J. Sel. Topics Quantum Electron.*, 12:1688–1698.

Lee, M., Rucker, H., and Choi, W. (2012). Effects of guard-ring structures on the performance of silicon avalanche photodetectors fabricated with standard cmos technology. *IEEE Electron Devices Letters*, 33:80–83.

Saveliev, V. (2010). *Silicon Photomultipliers, new era of photon detection*. In: Ed. K.Y. Kim, Advances in Optical and Photonic Devices, Intech, ISBN: 978-953-7619-76-3, 1st edition.

Saveliev, V. and Golovin, V. (2000). Silicon avalanche photodiodes in base metal resistor semiconductor (mrs) structures. *Nuclear instruments and methods A*, 442:223–229.

Silvaco. http://www.silvaco.com.

Sze, S. and K.N., N. (2007). *Physics of Semiconductor Devices*. Wiley, 3st edition.

Zappa, F., Tisa, S., Tosi, A., and Cova, S. (2007). Principles and features of single-photon avalanche diode arrays. *Sensors and acuators A - physical*, 140:103–112.